Bayesian Markov-chain-Monte-Carlo inversion of time-lapse crosshole ground-penetrating radar data to characterize the vadose zone at the Arrenaes field site, Denmark

Marie Scholer[1], James Irving[1*], Majken C. Looms[2], Lars Nielsen[2] and Klaus Holliger[1]

[1] Institute of Geophysics, University of Lausanne,

CH-1015 Lausanne, Switzerland

[2] Department of Geography and Geology, University of Copenhagen,

DK-1350 Copenhagen, Denmark

[*] Corresponding author: james.irving@unil.ch

Manuscript for *Vadose Zone Journal*

29 March 2021

Abstract

The ground-penetrating radar (GPR) geophysical method has the potential to provide valuable information on the hydraulic properties of the vadose zone because of its strong sensitivity to soil water content. In particular, recent evidence has suggested that the stochastic inversion of crosshole GPR traveltime data, which contain detailed information about the spatial distribution of water content at the field scale, can allow for a significant reduction in uncertainty regarding subsurface van-Genuchten-Mualem (VGM) parameters. Much of the previous work on the stochastic estimation of VGM parameters from crosshole GPR traveltime data has considered the case of steady-state infiltration conditions, which represent only a small fraction of practically relevant scenarios. Here, we explore in detail the dynamic infiltration case, specifically examining to what extent time-lapse zero-offset-profile crosshole GPR traveltimes, measured during a forced infiltration experiment at the Arreneas field site in Denmark, can help to quantify VGM parameters and their uncertainties in a layered medium, as well as the corresponding soil water retention curves and unsaturated hydraulic conductivity functions. To do this, we use a Bayesian Markov-chain-Monte-Carlo (MCMC) stochastic inversion approach. We first explore the advantages and limitations of this approach with regard to a representative and realistic synthetic example before applying it to field measurements. In our analysis, we also consider the effects of different degrees of prior information on the posterior results. Our findings indicate that the stochastic inversion of the time-lapse GPR traveltime data does indeed allow for a substantial refinement in the inferred posterior VGM parameter distributions compared to the corresponding priors, which in turn significantly improves knowledge of the soil hydraulic properties. Overall, the results obtained in our work therefore clearly demonstrate the value of the information contained in time-lapse GPR traveltime data for characterizing vadose zone dynamics.

1. Introduction

Accurate modeling of vadose zone flow and transport processes requires detailed knowledge of subsurface unsaturated hydraulic properties, namely the soil water retention curve and hydraulic conductivity function. Traditionally, such information is obtained using a variety of methods ranging from laboratory tests on representative samples from the field to *in situ* monitoring techniques involving tensiometer, time-domain reflectometry (TDR), and/or neutron probe measurements (e.g., Smith and Mullins, 1991). A critical drawback of all of these methods is their small support volume; that is, being made at essentially the point scale, the corresponding measurements are subject to significant variability and may not adequately represent larger-scale vadose zone processes (e.g., Binley et al., 2002). Geophysical methods, such as ground-penetrating radar (GPR) and electrical resistivity tomography (ERT), have gained much interest in hydrology as they allow for the estimation of subsurface properties at a larger, more relevant integral scale (e.g., Hubbard and Rubin, 2005). A trade-off associated with the use of such methods in a hydrological context, however, is that they are sensitive to, and therefore give us information regarding, geophysical properties in the subsurface and not directly the hydrological properties of interest. It is well known that petrophysical relationships between geophysical quantities and those controlling flow and transport tend to be site-specific, non-unique, and extremely difficult to establish (e.g., Day-Lewis et al., 2005).

One increasingly popular means of dealing with the above issue, and thus making more effective use of geophysical methods for subsurface hydraulic property estimation, involves first connecting the geophysical data with one or more hydrological state variables, such as water content or solute concentration, to which the data are sensitive and linked in a well established manner. Knowledge of the state variables, combined with a process-based hydrological model, can then be used to infer values for the governing hydraulic properties (e.g., Kemna et al., 2002; Day-Lewis et al., 2003; Singha and Gorelick, 2005). In this regard,

direct coupling of the geophysical and hydrological models, where the numerical models for the geophysical and hydrological processes are linked together such that the geophysical data are inverted directly for the hydraulic properties of interest, is often preferred to separated or uncoupled inversion (e.g., Rucker and Ferre, 2004; Lambot et al., 2006; Looms et al., 2008a) because it avoids issues related to the formation of geophysical images and their dependence upon the style and amount of regularization used, which can significantly affect the hydrological estimates obtained (e.g., Day-Lewis et al., 2005). Stochastic inversion approaches are also being employed with increasing frequency in such work because the corresponding problems tend to be highly non-linear and difficult to address with deterministic methods (e.g., Kowalsky et al., 2004, 2005; Hinnell et al., 2010; Irving and Singha, 2010). Moreover, stochastic inverse methods readily allow for the assessment of uncertainty in the estimated hydraulic parameters, which is critical for the evaluation of risk and the development of effective management and/or remediation strategies.

In an attempt to quantify vadose zone hydraulic properties *in situ* at the field scale, a number of researchers have recently investigated the stochastic inversion of crosshole GPR traveltime data within the above framework. Specifically, by linking these data first to subsurface water content, a state variable upon which the GPR measurements are strongly dependent and connected in a relatively straightforward manner, the estimation of unsaturated hydraulic properties can be performed using a model for infiltration. Binley and Beven (2003), for example, used zero-offset-profile (ZOP) crosshole GPR traveltime data to constrain the changes in moisture content caused by natural loading in the vadose zone during a two-year monitoring period. Assuming a 1D layered subsurface and steady-state infiltration conditions, as justified by the observational evidence, the GPR-derived moisture content profiles were then considered in a pseudo-Bayesian Generalized Likelihood Uncertainty Estimation (GLUE) inversion strategy to identify “behavioral” sets of van-Genuchten-

Mualem (VGM) parameters (Mualem, 1976; van Genuchten, 1980) that all fit the data to within a prescribed degree of uncertainty. Binley et al. (2004) and Cassiani and Binley (2005) built on this work and used a similar inversion strategy to estimate the VGM parameters in a layered medium under steady-state conditions where the layer boundaries were stochastically defined. In all of these studies, only field data were considered and broad uniform prior parameter distributions were assumed. Although the corresponding results did show a slight improvement in the estimation of the VGM parameters through the incorporation of the geophysical data, the benefits were marginal and unequivocal estimation of the parameters was not possible. Further, without synthetic testing, it was not possible to truly validate the effectiveness of the proposed methodologies. Recently, Scholer et al. (2011) examined the steady-state infiltration problem of Cassiani and Binley (2005) in further detail, testing on both synthetic and field GPR traveltime data whether a formal Bayesian Markov-chain-Monte-Carlo (MCMC) inversion approach could be used to successfully reduce uncertainty regarding the VGM parameters in a layered subsurface medium. Quite importantly, their study also explored the effects of different prior parameter distributions, which ranged from uniform and non-informative to more realistic, informed priors derived from soil property databases. The analysis of Scholer et al. (2011) clearly demonstrated that the considered GPR traveltime data contained valuable information regarding the VGM parameters in each subsurface layer. Further, significantly better results were obtained when the data were combined with a realistic, informative prior in the stochastic inversion procedure. Similar conclusions were drawn by Mertens et al. (2004) and Scharnagl et al. (2011), who inverted TDR water content measurements for soil VGM parameters and also investigated the impact of different priors on the estimated posterior parameter distributions. For excellent summaries of this and other works on the inversion for soil hydraulic properties in a non-geophysical context, see the recent papers of Scharnagl et al. (2011) and Wöhling and Vrugt (2011).

In this paper, we extend the research of Scholer et al. (2011) and investigate the use of time-lapse ZOP crosshole GPR traveltime data to estimate the VGM parameters in a layered subsurface medium for the case where steady-state infiltration conditions cannot be assumed. Indeed, steady-state conditions are the exception, rather than the norm, in the vadose zone and thus consideration of the dynamic infiltration case is critical (Nimmo, 2005). Further, dynamic measurements have the potential to significantly improve VGM parameter estimates past the steady-state case because they provide a means of monitoring infiltration behavior through a range of water content values (e.g., Binley and Beven, 2003). To this end, we explore the application of a Bayesian MCMC stochastic inversion strategy to time-lapse crosshole GPR traveltime data acquired by Looms et al. (2008b) over the course of a forced infiltration experiment at the Arrenaes field site in Denmark. Looms et al. (2008a) already performed a preliminary stochastic exploration of these data using a GLUE-type inversion approach, which involved examination of the misfits of ~4000 random VGM parameter configurations drawn from broad uniform distributions. Contrary to their expectations, however, the corresponding findings were largely inconclusive with regard to the value of the dynamic GPR traveltime data for constraining the VGM parameters and improving predictions of unsaturated hydraulic behavior. Hence our goal in this paper is to consider their database in further detail, and in particular to determine whether greater clarity on this issue can be obtained through (i) the use of a formal Bayesian inference methodology; (ii) more efficient and comprehensive exploration of the posterior model parameter space through MCMC sampling and the consideration of a significantly greater number of model parameter realizations; (iii) extensive testing on realistic and representative synthetic data; and (iv) investigating the effect of incorporating different degrees of prior information into the inversion procedure. We also extend the work of Scholer et al. (2011) by assessing all

inversion results not only in terms of the posterior VGM parameter distributions, but also in terms of the corresponding water retention and unsaturated hydraulic conductivity functions.

In the following, we first describe the hydrological and geophysical forward models and Bayesian MCMC inversion methodology employed in this work. Next, we provide details on the Arrenaes field site and forced infiltration experiment that was conducted there, along with the time-lapse crosshole GPR traveltime measurements that were acquired during infiltration. Within a synthetic example mimicking the Arrenaes field site, we then examine to what extent the time-lapse GPR traveltime data allow us to estimate the VGM parameters in the subsurface in the case of three different degrees of prior information, as well as to refine the corresponding water retention and unsaturated hydraulic conductivity functions. Finally, we apply the same analysis methodology to the field data collected at the Arrenaes site.

2. Methodology

2.1 Geophysical and hydrological models

In order to estimate subsurface VGM parameters from a set of crosshole GPR traveltime measurements, we require a link between the VGM parameters and the traveltime data. The development of this link involves the coupling of geophysical and hydrological forward models through the state variable water content. Scholer et al. (2011) describe this link for the steady-state infiltration case assuming 1D vertical flow. Building on their work to now consider dynamic conditions, we have as our governing hydrological process model the following form of Richards' equation (Richards, 1931) describing 1D variably saturated flow in porous media:

$$\frac{\partial}{\partial z}\left[K(h)\frac{\partial h}{\partial z}+K(h)\right]=\frac{\partial \theta(h)}{\partial t}, \tag{1}$$

where K is the unsaturated hydraulic conductivity, h is the pressure head, θ is the water content, z is depth, and t is time. With the VGM model (Mualem, 1976; van Genuchten,

1980), the water retention, expressed in terms of effective saturation S_e (dimensionless), is given by:

$$S_e(h) = \frac{\theta(h) - \theta_r}{\theta_s - \theta_r} = \begin{cases} (1 + |\alpha h|^n)^{-m} & \text{for } h \leq 0 \\ 1 & \text{for } h > 0 \end{cases} \quad (2)$$

where θ_r and θ_s are the residual and saturated water contents, respectively, and α, m, and n are empirical shape factors with $m = 1\text{-}1/n$. The unsaturated hydraulic conductivity as a function of pressure head is then given by

$$K(h) = K_s S_e(h)^{1/2} \left[1 - \left(1 - S_e(h)^{1/m} \right)^m \right]^2, \quad (3)$$

where K_s is the saturated hydraulic conductivity. A total of five model parameters, θ_s, θ_r, α, Ks, and n, therefore describe the soil hydraulic properties with the VGM model.

To solve equation (1) for the time-varying, 1D water content distribution during infiltration corresponding to a given set of subsurface VGM parameters and specified boundary and initial conditions, we use the program HYDRUS-1D (Simunek et al., 2008), which is based on a Galerkin-type linear finite-element scheme and is capable of dealing with an arbitrary number of subsurface layers. To link the resulting water content data to a set of crosshole GPR traveltimes, we then determine the soil relative dielectric permittivity, ε_r, versus depth for each measurement time using the Topp equation (Topp et al., 1980):

$$\varepsilon_r = 3.03 + 9.3\theta + 146\theta^2 - 76.7\theta^3. \quad (4)$$

Our use of the Topp equation is consistent with the work of Looms et al. (2008a), who found that it provides an adequate petrophysical link between water content and dielectric permittivity for the high-porosity soils at the Arrenaes field site. Next, the different profiles of soil permittivity are transformed to GPR velocity, v, using the following high-frequency, low-loss approximation that is valid in most environments amenable to GPR wave propagation (e.g., Annan, 2005):

$$v = \frac{c}{\sqrt{\varepsilon_r}}, \tag{5}$$

where c is the free-space electromagnetic wave velocity. Finally, to determine the crosshole GPR traveltimes corresponding to the water content profile at a particular measurement time, we solve the eikonal equation for the corresponding 1D velocity field:

$$\left|\nabla T(\mathbf{r})\right|^2 = s(\mathbf{r})^2 \tag{6}$$

where T is the traveltime of first-arriving energy from the transmitter antenna to the receiver antenna at location $\mathbf{r}$ through the slowness field $s(\mathbf{r})=1/v(\mathbf{r})$. For ZOP measurements, the antennas are placed at the same depth in two adjacent boreholes and the traveltime between them is determined versus depth. We solve equation (6) using a MATLAB version of the PRONTO eikonal software of Aldridge and Oldenburg (1993), which accounts for bending of the radar wavefront at interfaces across which velocities change. Indeed, the 1D water content profiles cannot be simply converted to traveltime by assuming the purely horizontal propagation of radar energy (Rucker and Ferré, 2004).

2.2 Bayesian MCMC inversion

As outlined earlier, we employ a Bayesian MCMC inversion approach in this study to estimate subsurface VGM parameters from a given set of dynamic ZOP GPR traveltime measurements. In general notation, the use of Bayes' theorem to combine prior information regarding a set of model parameters with observed data in order to yield a posterior probability density function can be expressed as follows:

$$p(\mathbf{m}|\mathbf{d}_{\mathbf{obs}}) = \frac{p(\mathbf{d}_{\mathbf{obs}}|\mathbf{m})p(\mathbf{m})}{p(\mathbf{d}_{\mathbf{obs}})} \tag{7}$$

where vectors $\mathbf{m}$ and $\mathbf{d}_{\mathbf{obs}}$ represent the model parameters and data, respectively. The conditional distribution $p(\mathbf{d}_{\mathbf{obs}}|\mathbf{m})$ is known as the model likelihood and can be regarded as a

measure of how well a particular model fits the observed data. Under the assumption that the data residuals should be independent and identically normally distributed, $p(\mathbf{d}_{\mathbf{obs}}|\mathbf{m})$ is given by the following weighted least-squares misfit equation (Mosegaard and Tarantola, 1995):

$$p(\mathbf{d}_{\mathbf{obs}}|\mathbf{m}) = \frac{1}{\left(2\pi\sigma_r^2\right)^{N/2}} \exp\left[-\frac{(g(\mathbf{m}) - \mathbf{d}_{\mathbf{obs}})^T (g(\mathbf{m}) - \mathbf{d}_{\mathbf{obs}})}{2\sigma_r^2} \right], \tag{8}$$

where N is the number of data, σ_r is the estimated standard deviation of the residuals, and $g(\mathbf{m})$ represents the forward model linking $\mathbf{m}$ and $\mathbf{d}_{\mathbf{obs}}$. In our case, $g(\mathbf{m})$ corresponds to the previously described hydrological and geophysical models connecting the VGM parameters to a set of dynamic ZOP GPR traveltime measurements. The term $p(\mathbf{m})$ in equation (7) is the prior probability distribution for the model parameters, which expresses our uncertainty about these parameters before the data, for example the observed GPR traveltimes, have been taken into account (e.g., Curtis and Lomax, 2001; Scales and Tenorio, 2001). The marginal probability of the observed data, $p(\mathbf{d}_{\mathbf{obs}})$, in equation (7) can be regarded as a normalization constant that ensures that the posterior probability distribution integrates to unity (e.g., Tarantola, 2005).

Because of the complexity of the forward models in most geophysical and hydrological problems, obtaining an analytical expression for the Bayesian posterior probability distribution in equation (7), and its associated moments, is generally not possible. However, the equation provides us with a way of calculating the posterior probability of occurrence of a set of model parameters, which means that MCMC methods can be used to generate samples that are effectively "drawn" from this distribution. These samples can then be used to calculate posterior uncertainties and make predictions. Gilks et al. (1996) provide an excellent introduction to the MCMC approach, whereas Mosegaard and Tarantola (1995) describe its application to Bayesian geophysical inverse problems. In our case, we perform MCMC sampling from the Bayesian posterior distribution by first drawing a random set of

model parameters, **m**, from their prescribed prior distributions. This forms the starting point for the Markov chain. Next, a new set of model parameters, **m′**, is proposed, conditional on the current set **m**, by drawing from a proposal density function, $Q(\mathbf{m}'|\mathbf{m})$. In our work, $Q(\mathbf{m}'|\mathbf{m})$ is symmetric and defined to be a bounded uniform probability distribution centered on **m** whose width is chosen such that the size of the model perturbations allows for a reasonable rate, typically around 30%, of accepted transitions in the MCMC procedure (Gilks et al., 1996). Next, we decide whether or not to replace the current parameter set **m** with the proposed set **m′** using the Metropolis decision rule (Metropolis et al., 1953), for which the acceptance probability is given by:

$$P_{acc} = \min\left(1, \frac{p(\mathbf{m}')p(\mathbf{d}_{\mathbf{obs}}|\mathbf{m}')}{p(\mathbf{m})p(\mathbf{d}_{\mathbf{obs}}|\mathbf{m})}\right) \tag{9}$$

In other words, if the product of the prior and likelihood probabilities for the proposed set of model parameters is greater than that for the current set, the proposal is always accepted and the next step of the Markov chain becomes **m′**. If this is not the case, then the proposal is accepted with a probability equal to the ratio of the two products, which is practically achieved by drawing a random number $\alpha \in U(0,1)$ and accepting only if $\alpha < P_{\text{acc}}$. If the proposal is rejected, then the next step in the Markov chain is set to be the current model **m**. The process of proposing a perturbed set of model parameters and then accepting or rejecting is repeated to obtain successive samples in the Markov chain.

After an initial number of iterations, known as the burn-in period, the procedure outlined above can be proven to converge and generate samples from the Bayesian posterior distribution of model parameters. In other words, the Markov chain is guaranteed to eventually become independent of the starting values of the model parameters, and samples generated after this point can be collected and analyzed in terms of their posterior statistics. Hence, a first critical step in any application of MCMC methods is to determine the length of

the burn-in period. Unfortunately, there is no way to predict the number of burn-in iterations prior to running an MCMC inversion. As a result, a number of numerical tools for determining when burn-in has been achieved, which generally involve the calculation of metrics based on the outputs of a number of MCMC chains running in parallel, have been developed (e.g., Gelman and Rubin, 1992). Cowles and Carlin (1996) provide an excellent review of these methods. Another common and conceptually simpler means of estimating burn-in, which we implement in our work, involves visual inspection of the values of each model parameter versus iteration number for several parallel-running chains and assessing when the chains reach a similar equilibrium state (e.g., Gilks et al., 1996; Hassan et al., 2009).

Once burn-in has been reached and the samples from the Markov chain up to that point have been discarded, the next critical step in a Bayesian MCMC inversion is to determine the number of iterations that are required to generate enough statistically independent samples to properly characterize the posterior distribution. This will depend on the dimension of the model parameter space, the information content of the prior, and the degree of correlation between adjacent samples in the Markov chain that results from the bounded nature of the proposal density function. Indeed, if the posterior chain exhibits a long autocorrelation lag, then a greater number of iterations is required after burn-in to produce a sufficient number of independent posterior samples. We determine an appropriate length for the posterior Markov chain after burn-in using the strategy proposed by Gilks et al. (1996), which involves comparing ergodic averages for the various model parameters between a number of parallel-running chains and stopping when the averages are in good agreement.

3. Arrenaes field site and infiltration experiment

The Arrenaes field site in Denmark was developed to study flow and transport processes in the vadose zone (Looms et al., 2008b). Figures 1a and 1b show the location of this site and the

eight boreholes that have been installed there, respectively. Along each line of the cross indicated in Figure 1b, the outer two boreholes (7 m apart) were equipped for crosshole electrical measurements whereas the two inner boreholes (5 m apart) were intended for crosshole GPR measurements.

The water table at the Arrenaes site is located at approximately 30 m depth and the overlying sediments consist primarily of successive layers of alluvial sands with varying fractions of silt and clay (GEUS, 2011). Figure 1c shows a model of the layering of the sediments for the first 12 m, which were identified by Looms et al. (2008a) based on granulometric analyses of samples from a nearby well provided by Copenhagen Energy. The top, 1.75-m-thick, sediment layer consists of sandy clay, which is followed by a layer of coarse sand (~1.75 to ~4 m depth), a layer of finer sand (~4 to ~7.75 m depth), a thin layer of silt (~7.75 to ~8.25 m depth), and again coarse sand (~8.25 to ~12 m depth). In order to estimate *in situ* the VGM parameters of these five different layers at the field scale, Looms et al. (2008b) performed a forced infiltration experiment in the autumn of 2005, which they monitored with geophysical methods. Over a period of 20 days, ~95,000 liters of clean water were irrigated through 484 drippers over an area of ~7 x 7 m. During that time, 14 crosshole ERT and GPR data sets were collected. Here, we focus on the ZOP GPR traveltime measurements that were acquired between boreholes GPR1 and GPR3. These data were obtained using a Sensors and Software PulseEkko borehole radar system with 100 MHz antennae and a vertical antenna increment of 0.25 m in the interval between 1.5 and 12 m depth. This yielded 43 ZOP traveltime measurements per data set. The data were collected once per day until Day 10, after which they were collected on Days 13, 15, 17, and 20.

Figure 2a shows the various ZOP traveltime-versus-depth curves obtained during the Arrenaes infiltration experiment compared with the background curve acquired before the experiment began (Day 0). Notice the marked change in these curves with time over the

interval from ~1.5 to 8 m depth, which is caused by an overall increase in water content, and a corresponding increase of the GPR traveltime, due to infiltration. Below 8 m depth, however, the traveltime curves can be seen to undergo only minimal changes during the infiltration period. Because of the different hydraulic properties of the various layers, the high loading of the system, and the limited lateral extent of the infiltration domain, the flow induced by the forced infiltration experiment was not exclusively vertical. Indeed, a significant amount of the infiltrated water was diverted out of the area of interest as a result of lateral spreading at the silt layer interface at ~8 m depth. This is clearly seen in Figure 2b, which shows the calculated cumulative amount of water added to the subsurface volume over time based on the GPR traveltime data and assuming only 1D vertical flow. To create this figure, the traveltime curves in Figure 2a were first used to obtain profiles of water content versus depth using equations (4) and (5). The background water content profile for Day 0 was then subtracted from these data and the resulting difference profiles were integrated in depth to estimate the total amount of water added for that day. For the first five days, when the flow was indeed predominantly vertical, the increase in the calculated amount of added water in Figure 2b is seen to be linear. After Day 5, however, when the water front reached the silt layer and began to spread laterally, the calculated values are seen to fall short of this linear trend. Figure 2b also indicates that the calculated water accumulation rate over the course of the first five days of 0.0576 m/d is smaller than the infiltration rate of 0.0884 m/d used by Looms et al. (2008b) in the field. This is explained by the presence of clay in the uppermost 1.5 m of the soil profile, which resulted in additional lateral spreading of the infiltrated water near the surface.

To fully account for all of the above effects in a Bayesian MCMC analysis of the entire dynamic data set from the Arrenaes site, a 3D unsaturated flow model would be required. However, because of the computational expense of 3D flow simulations and the extremely large number of forward model calculations that are required for MCMC-based

inversions, this was not feasible. Indeed, when performing any stochastic inversion of geophysical or hydrological data, forward model accuracy must always be sacrificed to some degree for the sake of computational tractability (e.g., Irving and Singha, 2010). As a result, we chose to use a simpler 1D numerical flow model in this study to perform our inversions, and we consider only the GPR traveltime data from the first five measurement days,during which 1D vertical flow conditions prevail, as evidenced by the linear trend in Figure 2b. This provides us with a set of time-lapse geophysical data exhibiting large water content changes down to ~8 m depth and no significant water content changes below this depth. In addition, as an upper boundary condition for this 1D flow model, we consider an effective infiltration rate corresponding to that obtained from the GPR traveltime measurements under the assumption of purely vertical flow (Figure 2b), rather than the true infiltration rate from the field which is affected by lateral spreading near the surface.

4. Results

4.1 Synthetic feasibility study

4.1.1 Experiment and data

In the following, we consider a synthetic example closely based on the Arrenaes field case, wherein we perform the stochastic inversion of simulated time-lapse ZOP crosshole GPR traveltime data, which serve as a proxy for 1D water content dynamics, in order to estimate the subsurface VGM parameters and corresponding hydraulic properties. The consideration of a pertinent synthetic example allows us to assess the utility and information content of the GPR traveltime data for estimating the VGM parameters in the case where the parameter values are known and the boundary conditions can be strictly controlled. Table 1 shows the "true" VGM parameters that were assigned to each layer for this synthetic example assuming the same five-layer geological structure as at the Arreneas field site (Figure 1c). These values

were drawn from probability distributions for the corresponding materials derived by Carsel and Parrish (1988) from soil property databases. Please note that, although Layers 2, 3, and 5 at the Arrenaes field site are expected to be characterized by differing values of the VGM parameters, the corresponding layers in the synthetic example were assigned identical parameter values. This was done for simplicity and has no impact on our analysis, as the VGM parameters in each of the five layers were estimated separately in the Bayesian MCMC inversion procedure. Moreover, the use of identical parameter values for Layers 2, 3, and 5 allows us to compare how well the same hydraulic properties can be resolved at different depth levels.

To create a set of "observed" time-lapse ZOP GPR traveltime data corresponding to the "true" VGM parameter configuration described in Table 1, we first used a realistic unsaturated flow model to obtain the time-varying distribution of water content in the subsurface over the course of a synthetic infiltration experiment. To this end, the program VS2D (Lappala et al., 1987) was employed to solve Richards' equation in 2D cylindrical coordinates assuming radial symmetry about the z-axis. The use of VS2D instead of a 1D flow model like HYDRUS-1D allows us to adequately account for the lateral spreading observed in the Arrenaes field data, which provides a significant degree of realism for the synthetic example. Note, however, that, as mentioned previously, purely vertical infiltration was assumed in the subsequent Bayesian MCMC inversion procedure because running VS2D within this context was not computationally tractable. The considered simulation domain for the VS2D modeling was a cylinder of radius 7 m and height 30 m. The vertical and horizontal discretization intervals were set equal to 0.03 m and 0.15 m, respectively. The infiltration domain along the upper model boundary was limited to a circle of radius 3.6 m centered on the cylindrical symmetry axis, in order to yield a similar infiltration area to that used by Looms et al. (2008b) in the field. A constant input flux of 0.0884 m/d was prescribed over this

area, again to match the field experiment. The lower model boundary at 30 m depth was defined to be the water table. The two boreholes for the GPR measurements were considered to be located 5 m apart and in the center of the cylinder (i.e., at r = 2.5 m, φ = 0º and r = 2.5 m, φ = 180º).

After simulating infiltration over 20 days, the water content distributions obtained from VS2D were converted to GPR velocity using equations (4) and (5). We considered the same measurement times as in the field case, that is, one measurement per day until Day 10 and then subsequent measurements on Days 13, 15, 17 and 20. We then used the PRONTO eikonal equation solver with a grid discretization of 0.1 m to simulate the corresponding ZOP GPR traveltimes, and we added Gaussian random noise with a standard deviation equal to 1% of the mean traveltime to emulate more realistic conditions. Figure 3a shows the resulting synthetic time-lapse ZOP GPR traveltime curves, whereas Figure 3b shows the total amount of added water that was calculated as a function of time from these data using the same methodology as described previously. As expected, the traveltime profiles Figure 3a show less structure with depth than those in Figure 2a because the same VGM parameters used for Layers 2 and 3 in our synthetic example. In Figure 3b we see that, for the first 10 days of infiltration, the increase in the calculated amount of added water is seen to be linear, which indicates that flow through the subsurface is predominantly vertical. After Day 10, however, when the water front reaches the silt layer at 7.75 m depth, lateral spreading begins to occur which causes the calculated values to fall short of this linear trend. Because of this, we consider only the GPR traveltime data from the first 10 days of infiltration in our Bayesian MCMC analysis, where vertical, 1D flow conditions can be safely assumed and the use of HYDRUS-1D is justified. Also notice in Figure 3b that the calculated water accumulation rate of 0.0394 m/d over the first 10 days is smaller than the true infiltration rate of 0.0884 m/d, which is due to additional lateral spreading induced by the lower-permeability sediments near

the surface and necessitates modifying the upper boundary condition in the stochastic inversion procedure. The difference between the calculated and true infiltration rates is greater than that seen in Figure 2b, which suggests that the hydraulic parameters of Layer 1 in the synthetic example are representative of finer and less permeable sediments than those at the Arrenaes field site.

4.1.2 Prior distributions

As mentioned previously, Scholer et al. (2011) investigated the effects of different amounts of prior information in their Bayesian MCMC inversion of ZOP crosshole GPR traveltime data to estimate soil VGM parameters under steady-state conditions. This analysis was shown to be highly useful, as it helped not only to assess the information content of the traveltime data regarding the VGM parameters, but also to reveal what kind of information could be recovered from these data when they were combined with empirical prior information derived from soil property databases. In a similar fashion, we consider three different prior distributions when inverting the time-lapse GPR traveltime data in our synthetic example. These priors are specified for all of the VGM parameters except the saturated water content, θ_s, which is considered to be known and equal to 0.41 based on porosity measurements on core samples from the Arrenaes site (Looms et al., 2008a). Although fixing θ_s does neglect some of the uncertainty in soil hydraulic properties in the inversion procedure, it importantly allows us to compare our results with the previous work of Looms et al. (2008a) on the Arrenaes field data, who also considered θ_s as known. The three priors that we consider for the remaining VGM parameters, α, n, K_s, and θ_r, are the following:

1) The VGM parameters in each layer are assigned uniform prior distributions whose limits are defined in Table 2. The chosen bounds for these parameters are broad and consistent with previous work (e.g., Binley and Beven, 2003; Cassiani and Binley,

2005; Looms et al., 2008a; Scholer et al., 2011). More importantly, such broad, uniform priors allow us to assess the information with regard to the VGM parameters contributed by the GPR traveltime data alone. Note that the same uniform priors are considered for all of the subsurface layers in the MCMC inversion procedure, with the exception of θ_r, where we defined it to have a smaller uniform range in Layers 2-5 than in Layer 1, because this parameter must be smaller than the initial water content. Indeed, in the first layer, the initial water content was defined to be higher than in the other layers, which is consistent with observed soil water content profiles. Also note that the saturated hydraulic conductivity, K_s, is sampled in the $\log_{10}$ transformed space because of the inherently wide range of variability of this parameter.

2) The VGM parameters in each layer are assumed to follow empirical prior distributions as determined by Carsel and Parrish (1988) for the corresponding soil type based on the laboratory analysis of hundreds of different samples. Here, the prior sampling domain is significantly restricted when compared to the uniform priors, which allows us to assess how combining the GPR traveltime data with refined prior information affects estimation of the VGM parameters. In their work, Carsel and Parrish (1988) presented the empirical VGM parameter distributions in terms of a set of Johnson variable transformations (Johnson and Kotz, 1970), and the means, standard deviations, and correlation coefficients for the corresponding transformed, normally distributed variables. These data are shown in Table 3 for sand, silt, and sandy clay, which are the three soil types identified in the upper 12 m at the Arrenaes field site. We used this information to reconstruct the VGM parameter distributions for the three soil types, which were then used in equation (9) when deciding to accept or reject proposed transitions in the Bayesian MCMC procedure. In the case of this particular

refined prior, we assume that the VGM parameters are statistically uncorrelated and thus ignore the joint relationships provided by the correlation matrices in Table 3.

3) The VGM parameters in each layer are prescribed the same marginal prior statistics from Carsel and Parrish (1988) for the corresponding soil type as described above, but this time we even further restrict the sampling domain by including the full parameter correlation information provided in Table 3.

4.1.3 Bayesian MCMC inversion

The previously described Bayesian MCMC inversion methodology was used to estimate the VGM parameters in each of the five layers from the synthetic time-lapse ZOP GPR traveltime data shown in Figure 3a. Again, only the data from the first 10 days were considered, where infiltration could be safely assumed to be predominantly vertical. For the corresponding flow modeling with HYDRUS-1D, we used a vertical discretization interval of 0.03 m. The upper model boundary was set to the effective infiltration rate 0.0394 m/d, which was determined from the GPR traveltimes over the first 10 days (Figure 3b). Although this value is different from the actual infiltration rate of 0.0884 m/d used to create the synthetic data, it better represents the true vertical flow rate through the medium and thus provides consistently better estimates of the subsurface VGM parameters. The lower model boundary at 30 m depth was specified to be the water table. For the simulation of GPR traveltimes with the PRONTO eikonal equation solver, a spatial discretization of 0.1 m was used. The residual uncertainty term in equation (8) was set in accordance with the errors prescribed to the GPR traveltime data plus an estimated contribution related to model structural errors caused by our assumption of purely 1D flow. Three different Bayesian MCMC inversions were performed for each prior scenario using different random starting points. For the case of the uniform prior, burn-in was achieved after 50,000 iterations, and 200,000 iterations were determined to

adequately sample the posterior parameter space. In the case of both refined priors, burn-in was achieved after 20,000 iterations and only 125,000 subsequent iterations were necessary. The uniform and refined prior inversions took 10 and 7 days on a 3.16 GHz desktop computer, respectively.

Figure 4 shows the marginal prior and posterior histograms obtained for the different VGM parameters in each layer for the case of the uniform prior scenario. The true values of the parameters are also shown. Notice in this figure that, in many instances, the posterior distributions are noticeably more refined compared to the priors, which indicates that the time-lapse GPR traveltime data contain important information regarding the subsurface VGM parameters. Indeed, through the MCMC inversion of these data, we obtain significant reductions in uncertainty for K_s in each layer, and many smaller but still noticeable reductions in uncertainty for θ_r, n, and α. Also notice that the GPR traveltime data allow us to refine the VGM parameters in all of the layers, despite the fact that (i) there are no ZOP GPR traveltime data from 0 to 1.5 m depth, and (ii) the traveltime curves below ~8 m depth do not change over the first 10 days because the water has not yet infiltrated to this depth range (Figure 3a). Because the hydraulic properties of Layer 1 control how water is able to enter Layer 2, we are able to constrain these properties without actually having GPR measurements in Layer 1. In Layer 5, on the other hand, we see that although parameter refinement occurs through consideration of the GPR traveltime data, the true parameter values do not fall within the regions of high posterior probability as they do for the other layers where changes occur in the GPR traveltime data with time. Nevertheless, given the fact that water content does not change from the initial conditions in Layer 5, it is surprising that the GPR data provide us with any information. We believe that it is the fact that the water content does not change in Layer 5 over the 10-day period that allows us to constrain some of its hydraulic properties;

that is, knowing that this layer retains its initial water content over the 10 days provides us with information regarding the VGM parameters.

In Figure 5, we show the marginal prior and posterior histograms obtained for the VGM parameters in each layer for the case of the refined uncorrelated and correlated prior scenarios. Here we observe that the inclusion of more detailed prior information allows for a substantial reduction in uncertainty regarding the parameters compared to the case where uniform prior distributions were considered. Indeed, the posterior histograms in Figure 5 exhibit more clearly defined peaks than those in Figure 4 and there is much less ambiguity with respect to the true VGM parameter values in all layers, especially for n, θ_r, and α. Clearly, the refined priors of Carsel and Parrish (1988) provide a substantial amount of useful information to the inverse problem. Notice, however, that they do not provide us with everything, as evidenced by the marked improvement that occurs between many of the prior and posterior histograms in Figure 5. In other words, despite using significantly more refined priors in this case, we see that the GPR traveltime data still bring important additional information for constraining the subsurface hydraulic properties. Indeed, for the Bayesian MCMC inversion approach pursued in this study, it is the combination of the geophysical data with a refined, yet realistic, prior that yields the best results. In addition, note that using such refined priors helps to sample sets of VGM parameters that are consistent with the geological environment of interest, thus improving the efficiency of the stochastic inversion procedure by not testing unrealistic parameter combinations. Finally, notice in Figure 5 that the posterior distributions often change significantly between the uncorrelated and correlated cases. Including correlation in the prior provides better posterior estimates of the VGM parameters, which is consistent with recent work (e.g., Scharnagl et al., 2011; Scholer et al., 2011) and suggests that constraints on parameter correlation, if they are available, should be accounted for in Bayesian-type inversions for optimal results.

Figures 6 and 7 illustrate a more insightful way of quantifying how much benefit is brought to characterizing vadose zone hydraulic behavior through the inversion of the time-lapse ZOP GPR traveltime data in our synthetic example. Here, we examine the prior and posterior inversion results presented in Figures 4 and 5 in terms of the corresponding hydraulic properties (e.g., Scharnagl et al., 2011). In Figure 6, we show the soil water retention curves that were computed from the different sets of prior and posterior realizations. Figure 7 shows the corresponding unsaturated hydraulic conductivity functions. Note that these figures actually show the shaded density of the different prior and posterior curves plotted all together, such that regions with a white or yellow color in the figures represent places where a large number of prior or posterior curves overlap, respectively. We observe in Figures 6 and 7 that, for the case of the uniform prior, the posterior curves for Layers 2, 3, and 5 are significantly better constrained and centered around the true values than the prior curves, especially with regard to the water retention functions. These layers all correspond to sand having the same VGM parameters (Table 1). Notice, however, that the hydraulic behavior in Layer 5 is less well constrained by the GPR traveltime data than in Layers 2 and 3 because there is no corresponding variation in water content in this layer during the observation period. Also note for the case of the uniform prior that Layers 1 and 4, after consideration of the traveltime data, exhibit significantly different water retention behavior than Layers 2, 3 and 5, which confirms that these layers correspond to different soil types. All of this clearly demonstrates that the GPR traveltime data contain important information regarding the hydraulic behavior of each layer. When the refined priors are considered, a substantial further reduction in uncertainty is observed for the soil hydraulic properties. We now see that the posterior water retention curves and unsaturated hydraulic conductivity functions become closely centered around the true curves for all layers, and that the incorporation of the GPR traveltime data still brings important information. Regarding the uncorrelated and correlated

cases, we again observe that accounting for correlation between the VGM parameters in the prior helps to better refine the hydraulic behavior.

4.2 Inversion of the Arrenaes field data

We now apply the Bayesian MCMC inversion methodology to the time-lapse ZOP GPR traveltime data collected at the Arrenaes field site (Figure 2a). We ran the inversion procedure considering the same three priors that were used in the synthetic example (Tables 2 and 3). Again, the uniform priors, which were prescribed relatively broad bounds, allow us to assess the information content of the traveltime data with respect to the VGM parameters, whereas the refined priors based on the work of Carsel and Parrish (1988) allow us to examine how combining these data with empirical prior information can help to further constrain estimates of these parameters. For the inversions, the residual uncertainty term in equation (8) was again set in accordance with estimated errors on the GPR traveltime measurements of 0.4 ns (Looms et al., 2010) plus an estimated contribution from model structural errors. For each prior scenario, three independent parallel Markov chains with randomly chosen starting points were again initiated. A sufficient burn-in period for the field data was determined to be 60,000 iterations for the uniform prior and 20,000 iterations for both the uncorrelated and correlated refined priors. A total of 220,000 iterations for the uniform prior and 150,000 iterations for both refined priors were run for each parallel chain in order to properly sample the posterior parameter space. Running these inversions took 12 days and 8 days on the same 3.16 GHz desktop computer, respectively.

Figures 8 and 9 show the marginal prior and posterior histograms obtained for the different VGM parameters in each layer for the case of the uniform and refined prior distributions, respectively. In Figure 8 we see that, through the inversion of the time-lapse GPR traveltime data, the uncertainty in the VGM parameters in each layer is noticeably

reduced compared to the corresponding uniform prior distributions, which is consistent with our findings in the synthetic example. There are significant reductions in uncertainty for K_s and n, and smaller, but again still important, refinements for θ_r and α. The trends in K_s with depth seen in the posterior results are also consistent with observations of the grain size characteristics of the different soils (Figure 1) (Looms et al., 2008a). That is, the posterior values of K_s in Layers 2 and 3, which correspond to sand, are considerably higher than those in Layers 1 and 4, which contain signficant amounts of finer material and are thus expected to have a lower permeability (Figure 1). All of this indicates that the GPR traveltime data contain valuable information with regard to constraining the VGM parameters at the Arrenaes field site. It is important to note that, in their preliminary stochastic analysis of the Arrenaes data using similar uniform prior distributions for the VGM parameters, Looms et al. (2008a) found that they could also constrain K_s and n in Layers 1, 2 and 3, although to a lesser extent than is shown in Figure 8. Looms et al. (2008a) were not, however, able to constrain any of the other VGM parameters, nor could they see any refinement in these parameters in Layers 4 and 5, which led to a lack of clarity regarding the utility of the GPR traveltime measurements for constraining subsurface hydrological behavior. Through the use of a formalized Bayesian inversion framework with efficient MCMC sampling from the posterior distribution and consideration of a substantially greater number of model parameter realizations, we have significantly improved on these findings and are able to conclusively show the valuable information that is contained in the time-lapse GPR data regarding the VGM parameters at the Arrenaes site. This represents a substantial step forward.

For the case of the uncorrelated and correlated refined prior distributions, Figure 9 demonstrates that, as could be expected, we obtain a significant reduction in posterior uncertainty regarding all of the VGM parameters compared to the uniform prior case. However, as was found in the synthetic example, the GPR traveltime data still bring important

information to the inverse problem that is not contained in the refined priors. For example, Layers 2 and 3 were assigned the same refined prior distributions, corresponding to sand, in the Bayesian MCMC inversion procedure (Table 2). The resulting posterior distributions, however, clearly show lower values of K_s in Layer 3 than in Layer 2, which is consistent with the granulometric analysis of Looms et al. (2008a) that indicated the presence of finer, and thus less permeable, sand in Layer 3 than in Layer 2. Without the use of a refined, realistic, prior, this subtle differentiation between the sands in Layers 2 and 3 would not be possible in the context of the considered Bayesian MCMC inversion approach. Indeed, neither our work nor the previous work of Looms et al. (2008a) was able to identify this textural difference through the use of a uniform prior distribution. Additionally, we see in Figure 9 that accounting for parameter correlation in the inversion procedure further reduces our uncertainty regarding the VGM parameters as compared to the uncorrelated case.

Finally, we investigate how the soil hydraulic properties are refined for each of the different priors through the incorporation of the Arrenaes field data. Figure 10 shows the water retention curves for each layer corresponding to the three different prior and posterior parameter distributions shown in Figures 8 and 9, whereas Figure 11 shows the corresponding hydraulic conductivity functions. For the case of the uniform prior, we see that the curves generated from the posterior parameter realizations exhibit significantly more consistent behavior than the curves generated from the prior realizations. We also clearly observe that Layers 1 and 4 show strongly different hydraulic behavior than Layers 2, 3 and 5, which all show similar behavior that is typical for sand. Given the the fact that the same uniform priors were assumed for all layers, this again demonstrates that the GPR traveltime data contain important information regarding the hydraulic characteristics of the different soils at the Arrenaes field site. In the case of the uncorrelated refined prior distribution, we see a lesser reduction in uncertainty in the hydraulic properties between the prior and posterior compared

to the case of the correlated refined prior distribution. We also see in all cases more uncertainty in the water retention curves in Layer 5 than in Layers 2 and 3, because the water front does not reach Layer 5 over the considered infiltration period.

5. Discussion and Conclusions

We have demonstrated in this paper that time-lapse ZOP crosshole GPR traveltime data, collected while infiltration occurs so as to observe changes in subsurface water content, can be used to successfully constrain the hydraulic properties and behavior of the vadose zone through a stochastic inversion approach. This was done in the context of the forced infiltration experiment conducted by Looms et al. (2008b) at the Arrenaes field site using both synthetic and field data. Whereas the previous work of Looms et al. (2008a) involving the same field data and using a preliminary Monte-Carlo-type inversion approach yielded inconclusive results regarding the value of the GPR traveltime data for estimating VGM parameters, our analysis has clearly shown the pertinent information content of these data and their potential hydrological value. This in turn suggests that a formalized Bayesian inversion framework with efficient MCMC sampling from the posterior distribution represents a promising methodology for extracting key information from time-lapse geophysical data. Although our efforts in this study were focused on dynamic ZOP traveltime measurements acquired at the Arrenaes field site, the corresponding findings are likely to have general applicability to other types of geophysical data and field environments. We are currently investigating the use of crosshole ERT and multiple-offset-gather (MOG) GPR traveltime data from the Arrenaes field site in this regard.

Our consideration of different degrees of prior information in the stochastic inverse problem allowed us to systematically investigate a number of important issues. First, through the use of non-informative uniform prior distributions for the VGM parameters in each

subsurface layer, we were able to assess the information content of the time-lapse GPR traveltime data. In both the synthetic and field cases, our analysis clearly showed that these data alone provide valuable information about the VGM parameters, most importantly regarding K_s. Secondly, through the use of more refined prior distributions based on soil property databases, we were able to examine how the information contained in the traveltime data could be best exploited when combined with realistic prior information within a Bayesian framework. In this case, we observed that the posterior parameter estimates and corresponding hydraulic behavior and predictions were significantly improved over the case where a uniform prior was considered. More importantly, subtle information that could not be revealed through the use of a uniform prior came to light when using the refined priors. In addition, we found that realistic parameter correlation, which is rarely used in the context of the prior information for Bayesian investigations, allowed the greatest reduction of uncertainty.

Despite the considerable success that we observed through the use of refined prior distributions in this study, it is important to keep in mind that considering such priors must be done with caution. Indeed, great care must be taken in order to ensure that the priors are not overly specific or unrealistic, such that posterior results become strongly biased. Although we feel that the priors derived from soil property databases such as the work of Carsel and Parrish (1988) or the ROSETTA soils database (Schaap et al., 2001; Scharnagl et al., 2011) can provide useful information about the VGM parameters in vadose zone investigations, it must be acknowledged that the scale of the core samples that are used to create such databases differs from the support volume of the GPR traveltime data. As a result, additional work regarding the suitability of such priors and their scale-dependence is required. Further, a preliminary stochastic analysis involving the use of non-informative prior information, as was done in our work, is generally highly recommended because it can demonstrate a clear

incompatibility between prior assumptions and the information contained in the considered geophysical data.

Another important and complementary aspect of the work presented in this paper is the investigation of the results not only in terms of the VGM parameters, which has been the focus of previous related research efforts in hydrogeophysics (e.g., Binley and Beven, 2003; Cassiani and Binley, 2005; Looms et al., 2008a; Scholer et al., 2011), but also in terms of the underlying hydraulic properties that actually determine the pertinent flow behavior. Although, clearly, the water retention curves and unsaturated hydraulic conductivity functions shown in Figures 6, 7, 10, and 11 were computed from the different sets of VGM parameters in each case, there is an important difference between examination of the parameters themselves and examination of these functions. Subtle changes in the distribution of one of the VGM parameters, for example, may have a significant impact on the hydraulic properties. Similarly, changes in the joint distribution of the different VGM parameters, which are not easily observed in histogram plots like Figures 4, 5, 8, and 9, may also have considerable impact on these properties. In both our synthetic and field examples, the inversion of the time-lapse GPR traveltime data significantly helped to characterize the water retention curves and unsaturated hydraulic conductivity functions in each subsurface layer. Indeed, even when using a uniform prior, we could identify distinct differences in hydraulic behavior between the layers.

Finally, a critical issue that should be discussed in the context of Bayesian investigations, and which was not thoroughly addressed in this study, is that of model error. As mentioned previously, when performing any stochastic inversion of geophysical or hydrological data, forward model accuracy must always be sacrificed to some degree for the sake of computational tractability. In general, this is accomplished through the use of reduced parameterizations and/or simplified forward models. In our case, for example, a 1D unsaturated flow model combined with a 5-layer subsurface parameterization were assumed

for the Arrenaes field site in the Bayesian MCMC inversion procedure. Clearly, these assumptions, in particular that of 1D flow, are an approximation of the true behavior, as evidenced by the lateral spreading that was seen to exist at layer interfaces in both our synthetic example and field application. Such model errors, if not properly accounted for, have the potential to strongly bias posterior parameter uncertainties and yield correspondingly unreliable results. Nevertheless, we were able to deal with these errors in our work to a reasonable degree through the use of an effective infiltration rate calculated from the GPR traveltime data, and by considering only those data that were acquired over a time period where infiltration was predominantly 1D. However, future work should definitely involve more detailed study of model errors, their effects on the posterior statistics obtained, and how they may be accounted for through the Bayesian likelihood function.

Acknowledgements

This research was supported by a grant from the Swiss National Science Foundation.

References

Aldridge, D. F., and D. W. Oldenburg. 1993. Two-dimensional tomographic inversion with finite-difference traveltimes. J. Seism. Explor. 2:257-274.

Annan, A. P. 2005. GPR Methods for Hydrogeological Studies. p. 185-213. *In* Y. Rubin and S. S. Hubbard (ed.) Hydrogeophysics. Springer Dordrecht, the Netherlands.

Binley, A. M., G. Cassiani, R. T. Middleton, and P. Winship. 2002. Vadose zone flow model parameterisation using cross-borehole radar and resistivity imaging. J. Hydrol. 267:147-159.

Binley, A. M., and K. J. Beven. 2003. Vadose zone flow model uncertainty as conditioned on geophysical data. Ground Water 41:119-127.

Binley, A. M., G. Cassiani, and P. Winship. 2004. Characterization of heterogeneity in unsaturated sandstone using borehole logs and cross-borehole tomography. p. 129-138. *In* J. S. Bridge and D. W. Hyndman (ed.) Aquifer Characterization SEPM Society for Sedimentary Geology, Tulsa, OK.

Carsel, R. F., and R. S. Parrish. 1988. Developping Joint Probability-Distributions of Soil-Water Retention Characteristics Water Resour. Res. 24:755-769.

Cassiani, G., and A. M. Binley. 2005. Modeling unsaturated flow in a layered formation under quasi-steady state conditions using geophysical data constraints. Adv. Water Resour. 28:467-477.

Cowles, M. K., and B. P. Carlin. 1996. Markov chain Monte Carlo convergence diagnostics: A comparative review. J. Am. Stat. Assoc. 91:883-904.

Curtis, A., and A. Lomax. 2001. Prior information, sampling distributions, and the curse of dimensionality. Geophysics 66:372-378.

Day-Lewis, F. D., J. W. Lane, J. M. Harris, and S. M. Gorelick. 2003. Time-lapse imaging of saline-tracer transport in fractured rock using difference-attenuation radar tomography. Water Resour. Res. 39:1290-1303.

Day-Lewis, F. D., K. Singha, and A. M. Binley. 2005. Applying petrophysical models to radar travel time and electrical resistivity tomograms: Resolution-dependent limitations. J. Geophys. Res.-Sol. Ea. 110:B08206.

Gelman, A., and D. B. Rubin. 1992. Inference from Iterative Simulation Using Multiple Sequences. Stat. Sci. 7:457-472.

GEUS. 2011. Jupiter database, http://geus.dk/.

Gilks, W. R., S. Richardson, and D. Spiegelhalter. 1996. Introducing Markov chain Monte Carlo. p. 1-19. *In* W. R. Gilks, S. Richardson and D. Spiegelhalter (ed.) Markov chain Monte Carlo in practice. Chapman&Hall/CRC, London.

Hassan, A. E., H. M. Bekhit, and J. B. Chapman. 2009. Using Markov Chain Monte Carlo to quantify parameter uncertainty and its effect on predictions of a groundwater flow model. Environ. Modell. Softw. 24:749-763.

Hillel, D. 2004. Introduction to environmental soil physics. Elsevier Science, USA.

Hinnell, A. C., T. P. A. Ferre, J. A. Vrugt, J. A. Huisman, S. Moysey, J. Rings, and M. B. Kowalsky. 2010. Improved extraction of hydrologic information from geophysical data through coupled hydrogeophysical inversion. Water Resour. Res. 46:W00D40.

Hubbard, S. S., and Y. Rubin. 2005. Introduction to Hydrogeophysics. Springer Netherlands.

Irving, J., and K. Singha. 2010. Stochastic inversion of tracer test and electrical geophysical data to estimate hydraulic conductivities. Water Resour. Res. 46:W11514.

Johnson, N. L., and S. Kotz. 1970. Distributions in Statistics: Continuous Univariate Distributions Houghton Miffin company, Boston.

Kemna, A., J. Vanderborght, B. Kulessa, and H. Vereecken. 2002. Imaging and characterisation of subsurface solute transport using electrical resistivity tomography (ERT) and equivalent transport models. J. Hydrol. 267:125-146.

Kowalsky, M. B., S. Finsterle, and Y. Rubin. 2004. Estimating flow parameter distributions using ground-penetrating radar and hydrological measurements during transient flow in the vadose zone. Adv. Water Resour. 27:583-599.

Kowalsky, M. B., S. Finsterle, J. Peterson, S. Hubbard, Y. Rubin, E. Majer, A. Ward, and G. Gee. 2005. Estimation of field-scale soil hydraulic and dielectric parameters through joint inversion of GPR and hydrological data. Water Resour. Res. 41:W11425.

Lambot, S., E. C. Slob, M. Vanclooster, and H. Vereecken. 2006. Closed loop GPR data inversion for soil hydraulic and electric property determination. Geophys. Res. Lett. 33: L21405, doi: 10.1029/2006GL027906.

Lappala, E., R. Healy, and E. Weeks. 1987. Documentation of computer program VS2D to solve the equations of fluid flow in variably saturated porous media. Water-Resour. Inves. Rep. 83:4099.

Looms, M. C., A. M. Binley, K. H. Jensen, L. Nielsen, and T. M. Hansen. 2008a. Identifying unsaturated hydraulic parameters using an integrated data fusion approach on cross-borehole geophysical data. Vadose Zone J. 7:238-248.

Looms, M. C., K. H. Jensen, A. M. Binley, and L. Nielsen. 2008b. Monitoring unsaturated flow and transport using cross-borehole geophysical methods. Vadose Zone J. 7:227-237.

Looms, M. C., T. M. Hansen, K. S. Cordua, L. Nielsen, K. H. Jensen, and A. Binley. 2010. Geostatistical inference using crosshole ground-penetrating radar. Geophysics 75:J29-J41.

Metropolis, N., A. W. Rosenbluth, M. N. Rosenbluth, A. H. Teller, and E. Teller. 1953. Equation of State Calculations by Fast Computing Machines. J. Chem. Phys. 21:1087-1092.

Mertens, J., H. Madsen, L. Feyen, D. Jacques, and J. Feyen. 2004. Including prior information in the estimation of effective soil parameters in unsaturated zone modelling. J. of. Hydrol. 294:251-269.

Mosegaard, K., and A. Tarantola. 1995. Monte Carlo sampling of solutions to inverse problems. J. Geophys. Res. 100:12431-12447.

Mualem, Y. 1976. A new model for predicting hydraulic conductivity of unsaturated porous-media. Water Resour. Res. 12:513-522.

Nimmo, J. R. 2005. Unsaturated zone flow process. p. 2299-2322. *In* M. G. Anderson and J. Bear (ed.) Encyclopedia of hydrological sciences: Part 13-Groundwater. Wiley, Chichester UK.

Richards, L. A. 1931. Capillary conduction of liquids through porous mediums. J. Appl. Phys. 1:318-333.

Rucker, D. F., and T. P. A. Ferre. 2004. Parameter estimation for soil hydraulic properties using zero-offset borehole radar: Analytical method. Soil Sci. Soc. Am. J. 68:1560-1567.

Scales, J. A., and L. Tenorio. 2001. Prior information and uncertainty in inverse problems. Geophysics 66:389-397.

Schaap, M. G., F. J. Leij, and M. T. van Genuchten. 2001. ROSETTA: a computer program for estimating soil hydraulic parameters with hierarchical pedotransfer functions. J. Hydrol. 251:163-176.

Scharling, M. 2010. DMI Technical report 99-12: Klimagrid Danmark, Nedbør, Lufttemperatur og potential fordampning 20*20 & 40*40 Km, metodebeskrivelse.

Scharnagl, B., J. A. Vrugt, H. Vereecken, and M. Herbst. 2011. Bayesian inverse modelling of in situ soil water dynamics: using prior information about the soil hydraulic properties. Hydrol. Earth Syst. Sci. Discuss. 8:2019-2063.

Scholer, M., J. Irving, A. Binley, and K. Holliger. 2011. Estimating vadose zone hydraulic properties using ground penetrating radar: The impact of prior information. Water Resour. Res. 47:W10512.

Simunek, J., M. T. van Genuchten, and M. Sejna. 2008. Development and applications of the HYDRUS and STANMOD software packages and related codes. Vadose Zone J. 7:587-600.

Singha, K., and S. M. Gorelick. 2005. Saline tracer visualized with three-dimensional electrical resistivity tomography: Field-scale spatial moment analysis. Water Resour. Res. 41:W05023.

Smith, K. A., and C. E. Mullins. 1991. Soil analysis. M. Dekker, New York.

Tarantola, A. 2005. Inverse Problem Theory and Methods for Model Parameter Estimation. SIAM, Philadelphia.

Topp, G. C., J. L. Davis, and A. P. Annan. 1980. Electromagnetic determination of soil-water content-measurement in coaxial transmission-lines. Water Resour. Res. 16:574-582.

van Genuchten, M. T. 1980. A Closed-form Equation for Predicting the Hydraulic Conductivity of Unsaturated Soils. Soil Sci. Soc. Am. J. 44:892-898.

TABLES

Table 1: VGM parameters prescribed to the different layers in the synthetic example.

	K_s (cm.h^{-1})	n	α (cm^{-1})	θ_s	θ_r
Layer 1 (sandy clay)	0.12	1.6	0.015	0.41	0.08
Layers 2, 3, and 5 (sand)	34.7	2.75	0.14	0.41	0.04
Layer 4 (silt)	0.17	1.5	0.02	0.41	0.05

Table 2: Upper and lower bounds of the prior uniform distributions assumed for the VGM parameters in the Bayesian MCMC inversion procedure.

Layer	VGM parameters	Lower bound	Upper bound
1	θ_r	0	0.1
	α (cm^{-1})	0	0.2
	n	1.1	4.81
	$Log_{10}(K_s$ ($cm.h^{-1}$))	-2	2
2-5	θ_r	0	0.06
	α (cm^{-1})	0	0.2
	n	1.1	4.81
	$Log_{10}(Ks$ ($cm.h^{-1}$))	-2	2

Table 3: Johnson transformation type and limits of variation, along with the means (μ), standard deviations (σ), and correlation matrices for the transformed VGM parameters as determined by Carsel and Parrish (1988) for sand, sandy clay, and silt. The log-normal and log-ratio Johnson variable transformations are defined in the bottom row of the table.

	Johnson transformation and limits of variation			μ	σ	**Correlation matrix**			
Sand		**A**	**B**			θ_r	α (cm^{-1})	n	K_s (cm.h^{-1})
θ_r	Log-normal			-0.12	0.224	1	0.12	-0.85	-0.51
α (cm^{-1})	Log-ratio	0	0.25	0.378	0.439		1	0.29	0.74
n	Log-normal			0.978	0.100			1	0.84
K_s (cm.h^{-1})	Log-ratio	0	70	-0.39	1.150				1
Silt						θ_r	α (cm^{-1})	n	K_s (cm.h^{-1})
θ_r	-			0.042	0.015	1	-0.20	-0.61	-0.20
α (cm^{-1})	-			0.017	0.006		1	0.55	0.98
n	-			1.38	0.037			1	0.46
K_s (cm.h^{-1})	Log-normal			-2.20	0.700				1
Sandy clay						θ_r	α (cm^{-1})	n	K_s (cm.h^{-1})
θ_r	Log-ratio	0	0.12	1.72	0.700	1	0.93	0.95	0.97
α (cm^{-1})	Log-normal			-3.77	0.563		1	0.93	0.92
n	Log-normal			0.202	0.078			1	0.93
K_s (cm.h^{-1})	Log-normal			-4.04	2.020				1

Log-normal Johnson variable transformation: $Y = \ln(X)$

Log-ratio Johnson variable transformation: $Y = \ln[(X-A)/(B-X)]$

FIGURES

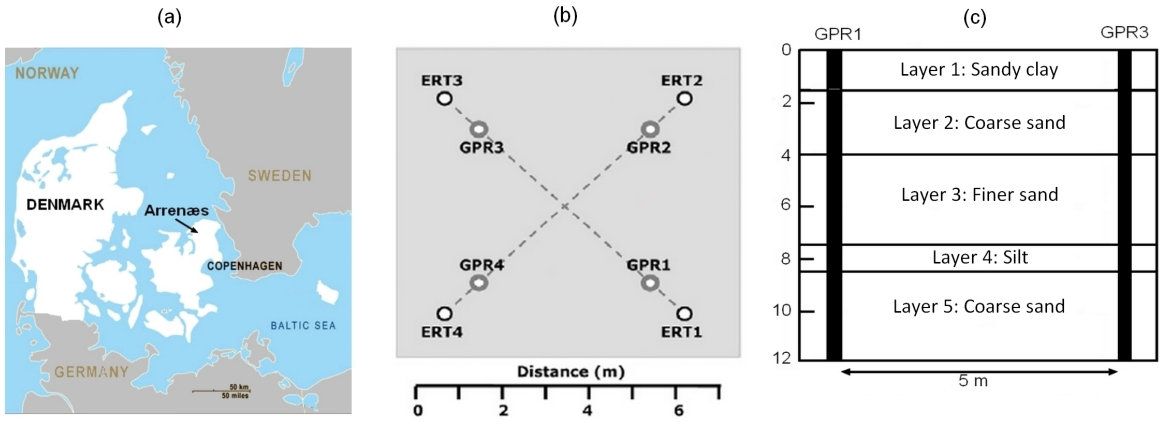

Figure 1: (a) Location of the Arrenaes field site, (b) the boreholes that have been installed there, and (c) the assumed layered geological structure in the study region. Modified from Looms et al. (2008b).

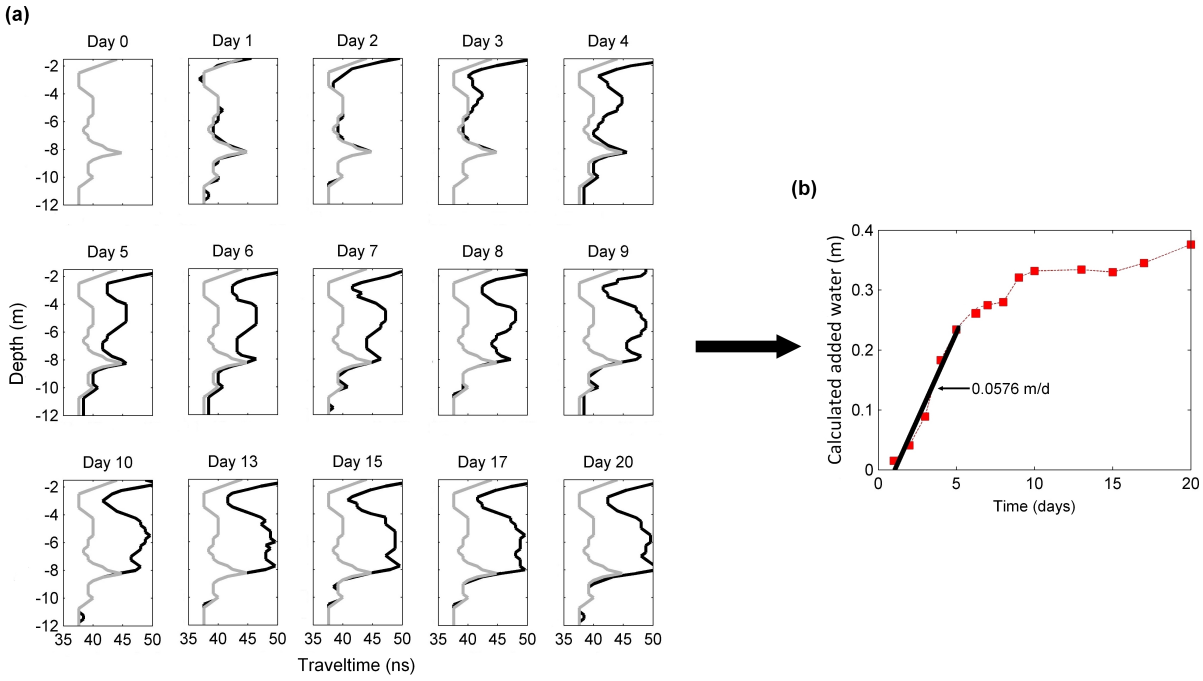

Figure 2: (a) ZOP crosshole GPR traveltime data acquired by Looms et al. (2008a) at the Arrenaes field site between boreholes GPR1 and GPR3 over the course of the 20-day infiltration experiment (black), compared with the traveltime data collected before infiltration began (grey). (b) Water added as a function of time calculated from the GPR data assuming 1D vertical flow. The black line shows the linear trend for the first 5 days.

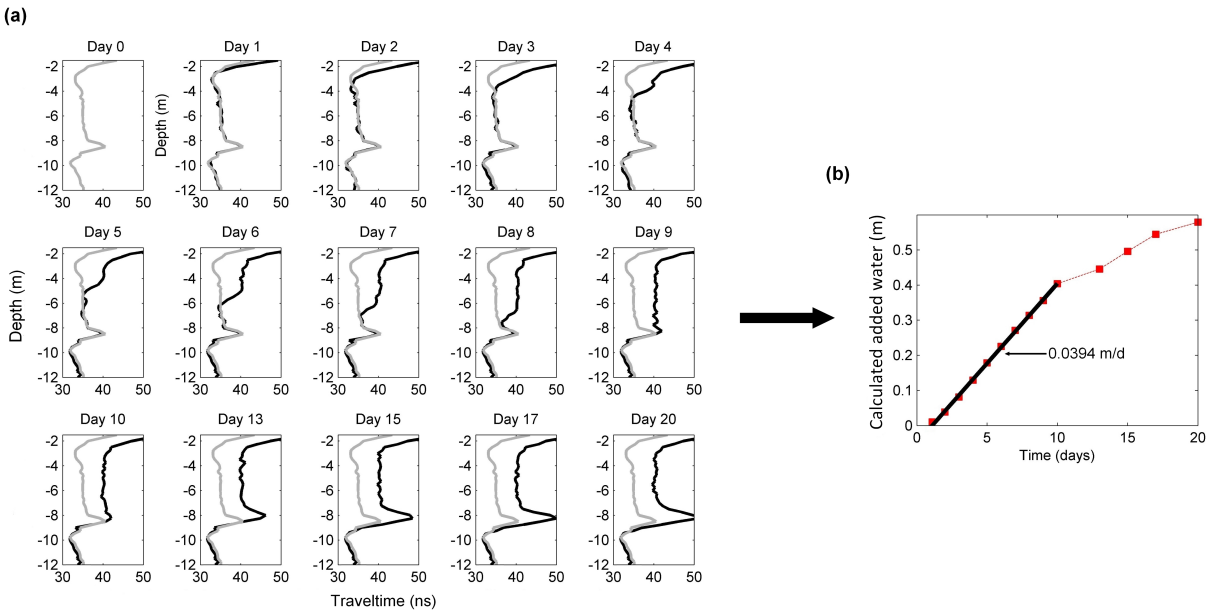

Figure 3: (a) Simulated time-lapse ZOP crosshole GPR traveltime data for the synthetic example (black), compared with the traveltime data that were simulated before infiltration began (grey). (b) Water added as a function of time calculated from the GPR data assuming 1D vertical flow. The black line shows the linear trend for the first 10 days.

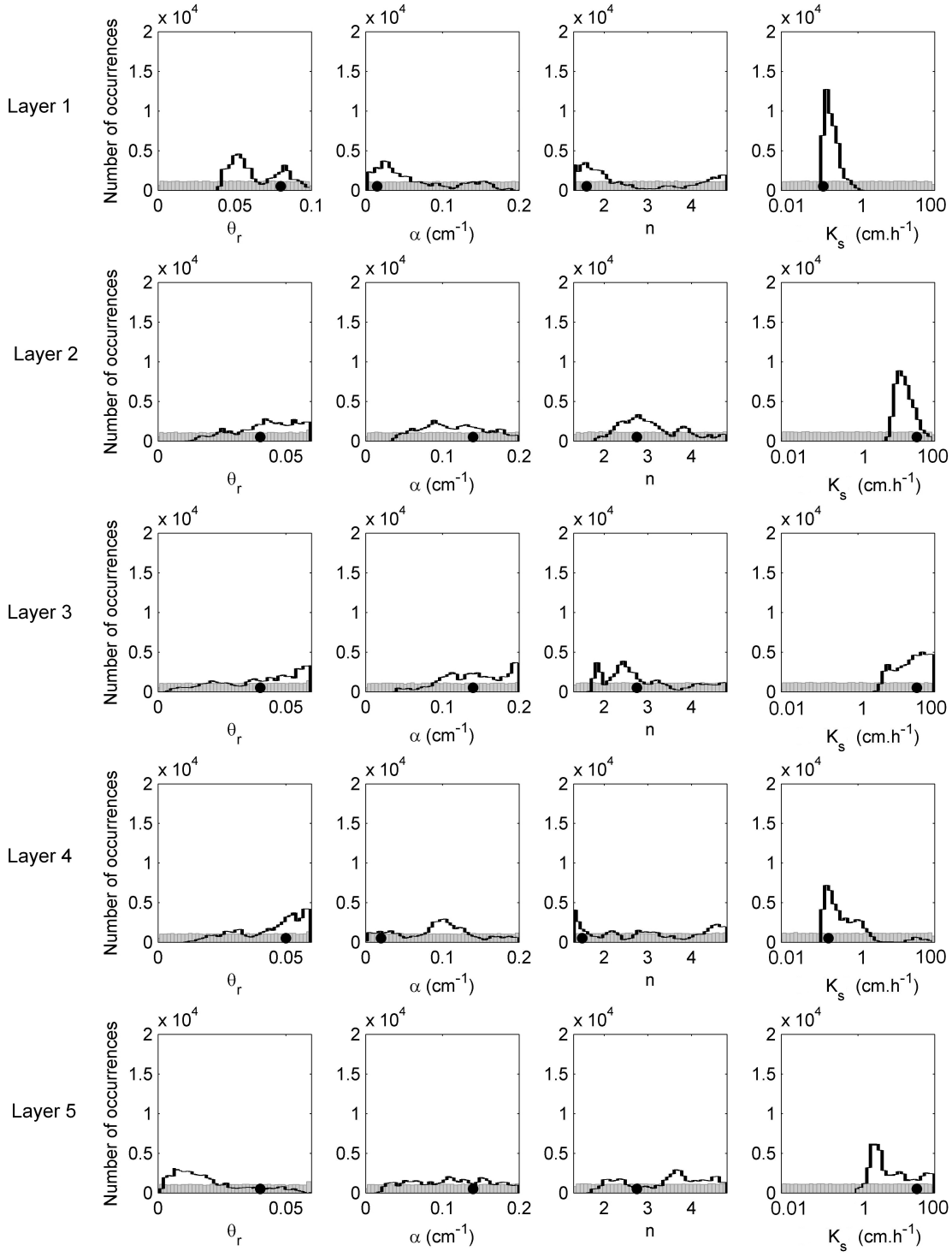

Figure 4: Uniform prior (grey) and corresponding posterior (black) histograms for the VGM parameters in each layer for the synthetic example. The black dots represent the true values.

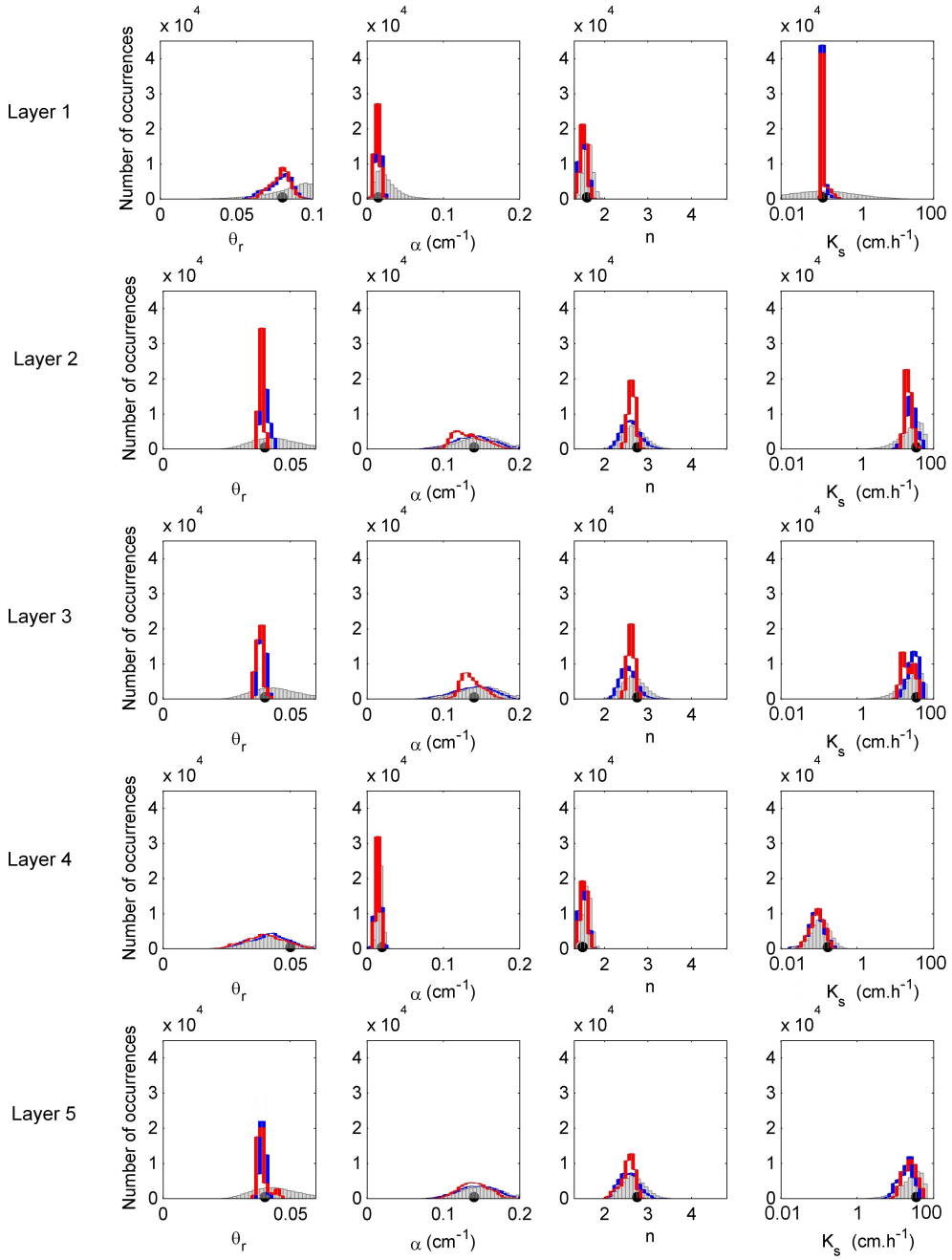

Figure 5: Refined prior (grey) and corresponding posterior histograms for the VGM parameters in each layer for the uncorrelated (blue) and correlated (red) scenarios for the synthetic example. The black dots represent the true values.

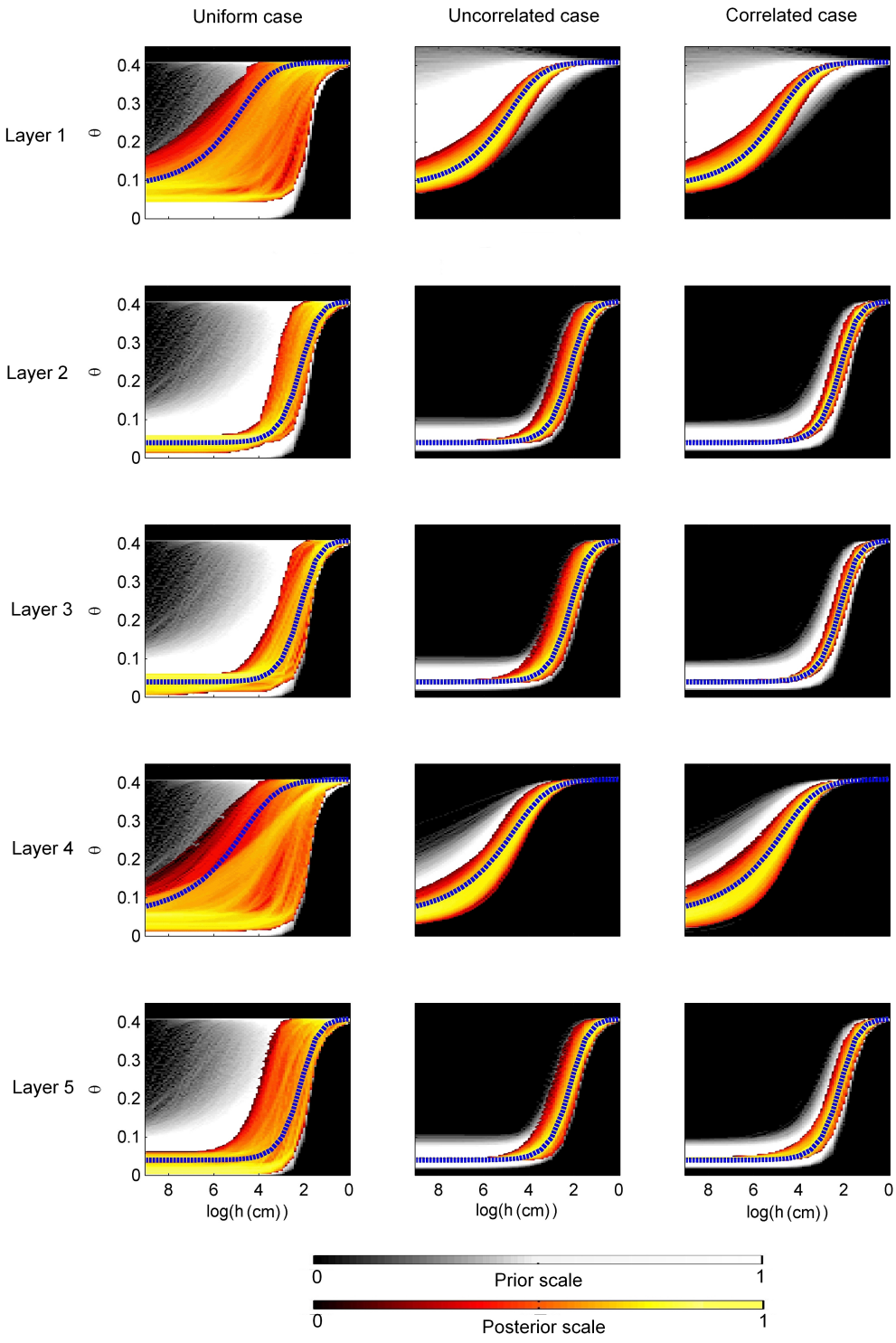

Figure 6: Water retention functions for each layer corresponding to the prior and posterior VGM parameter distributions shown in Figures 4 and 5. The true water retention functions are shown in blue.

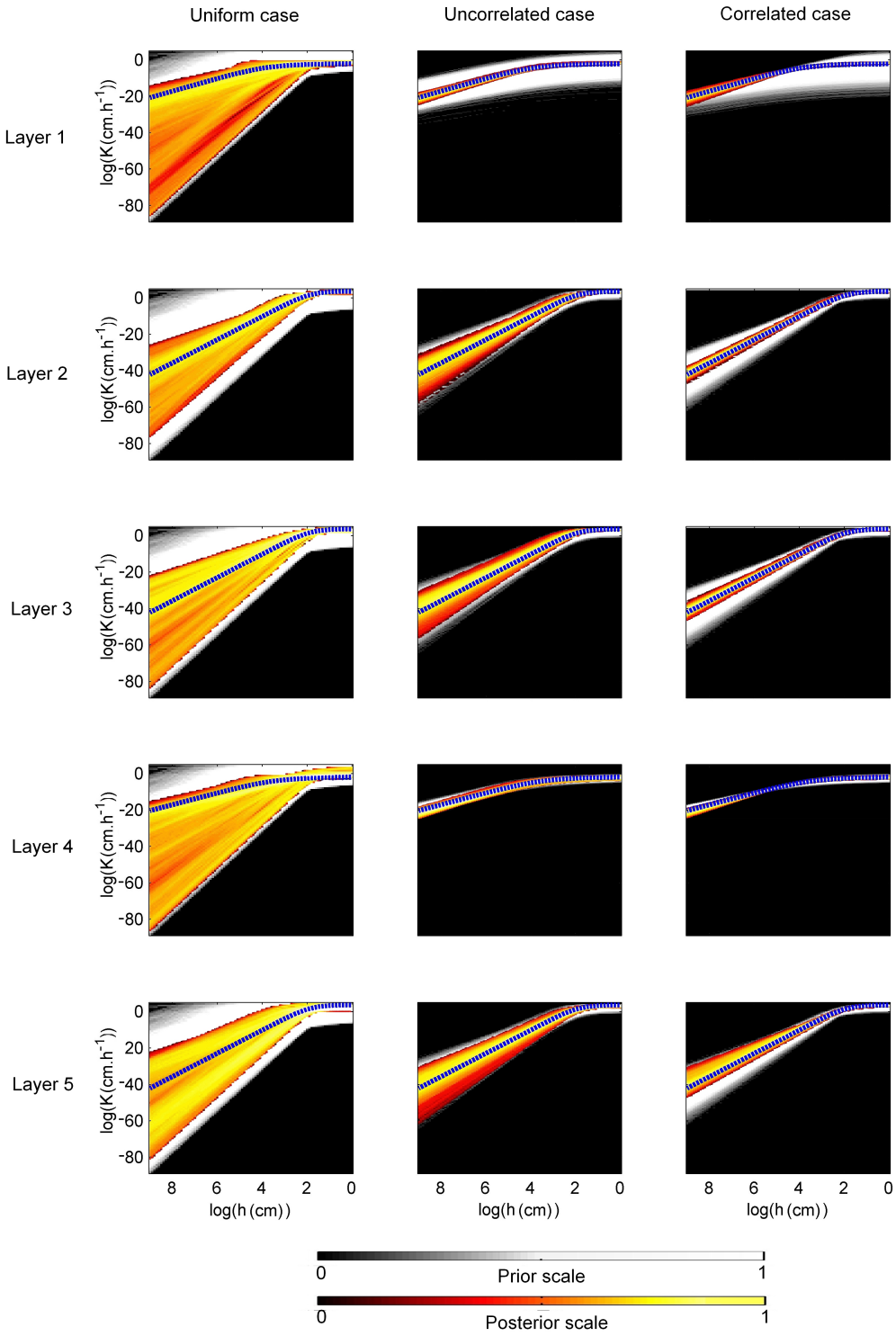

Figure 7: Hydraulic conductivity functions for each layer corresponding to the prior and posterior VGM parameter distributions shown in Figures 4 and 5. The true hydraulic conductivity functions are shown in blue.

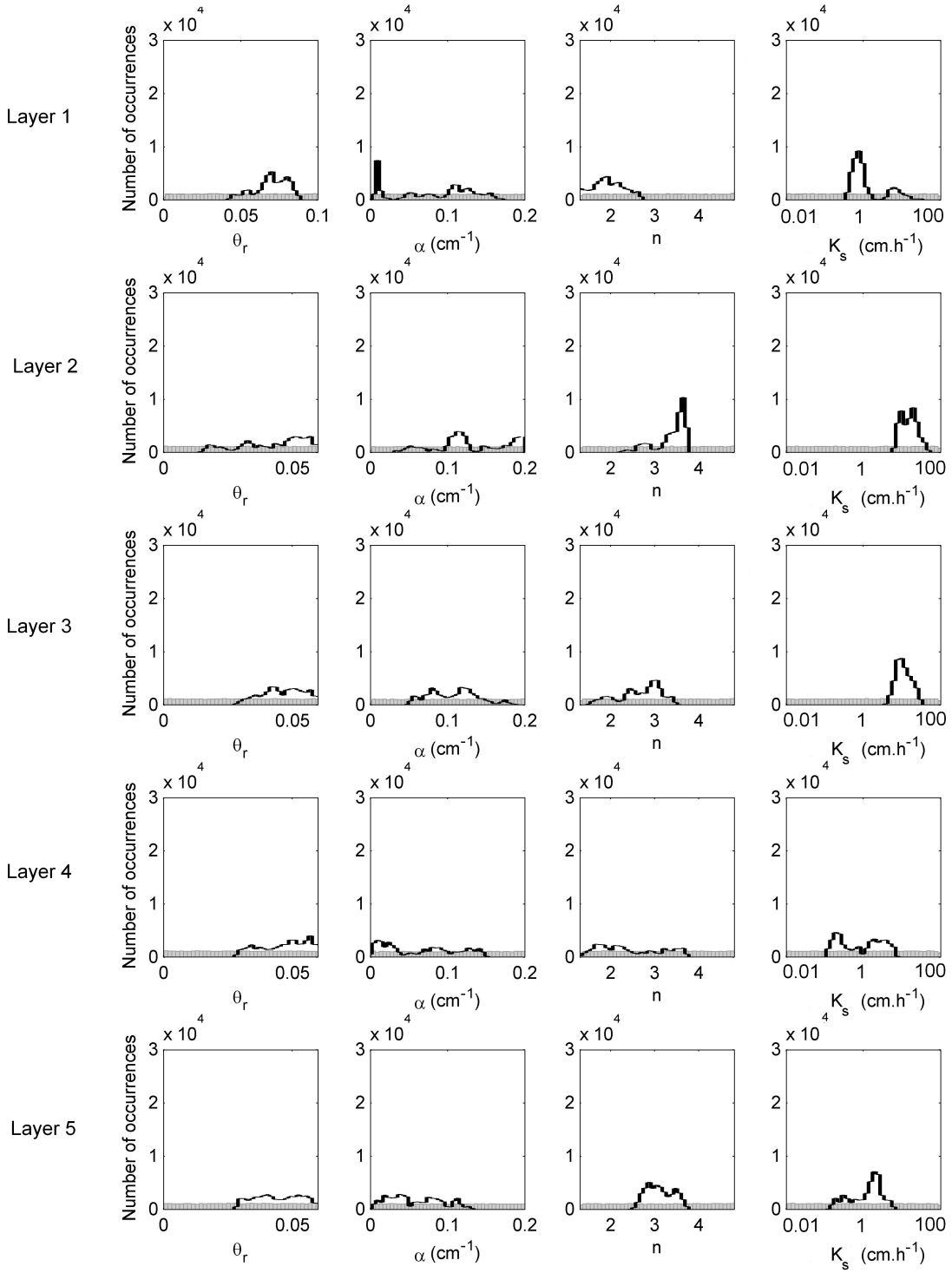

Figure 8: Uniform prior (grey) and corresponding posterior (black) histograms for the VGM parameters in each layer for the case of the Arrenaes field data.

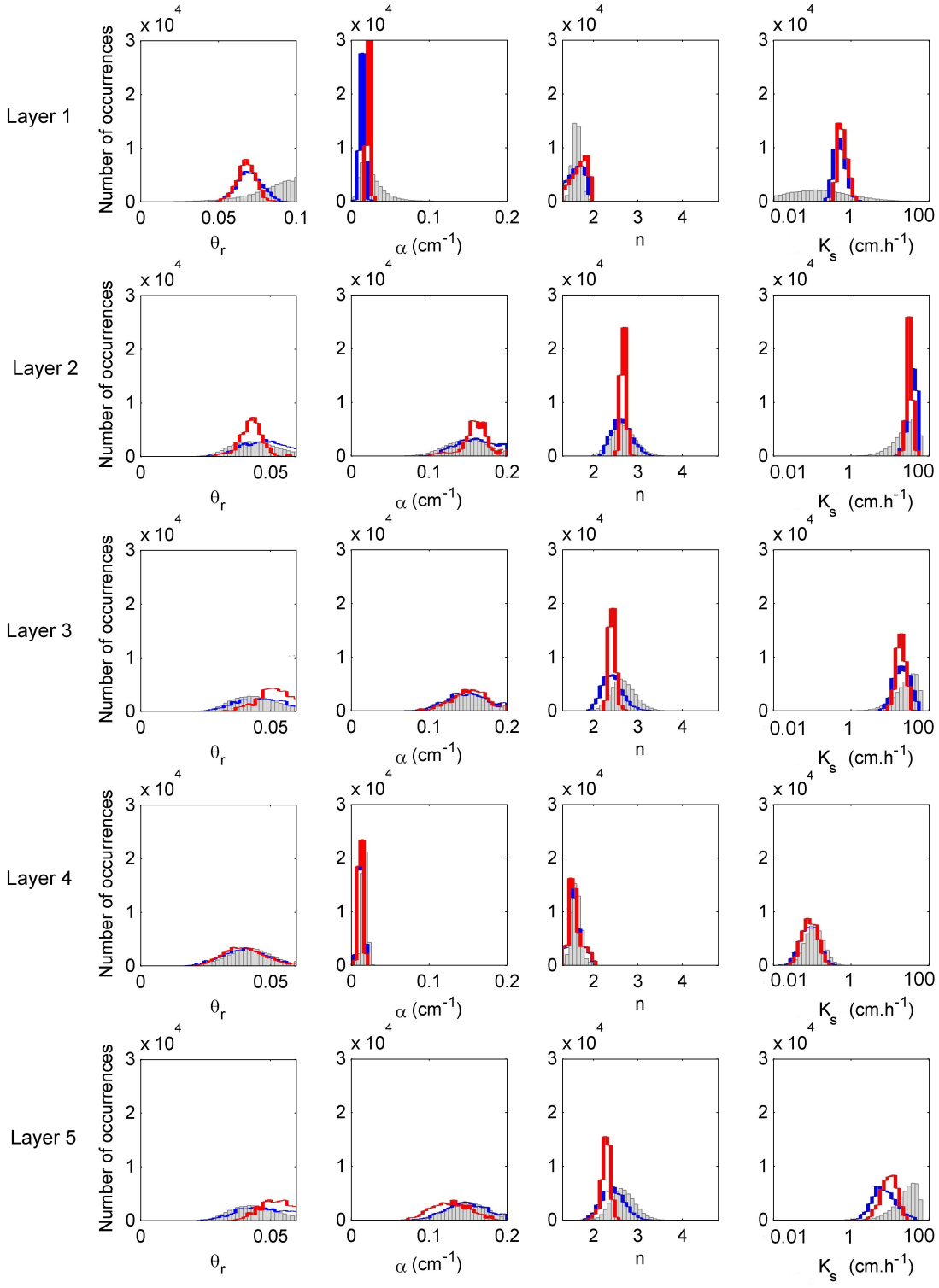

Figure 9: Refined prior (grey) and corresponding posterior histograms for the VGM parameters in each layer for the uncorrelated (blue) and correlated (red) scenarios for the case of the Arrenaes field data.

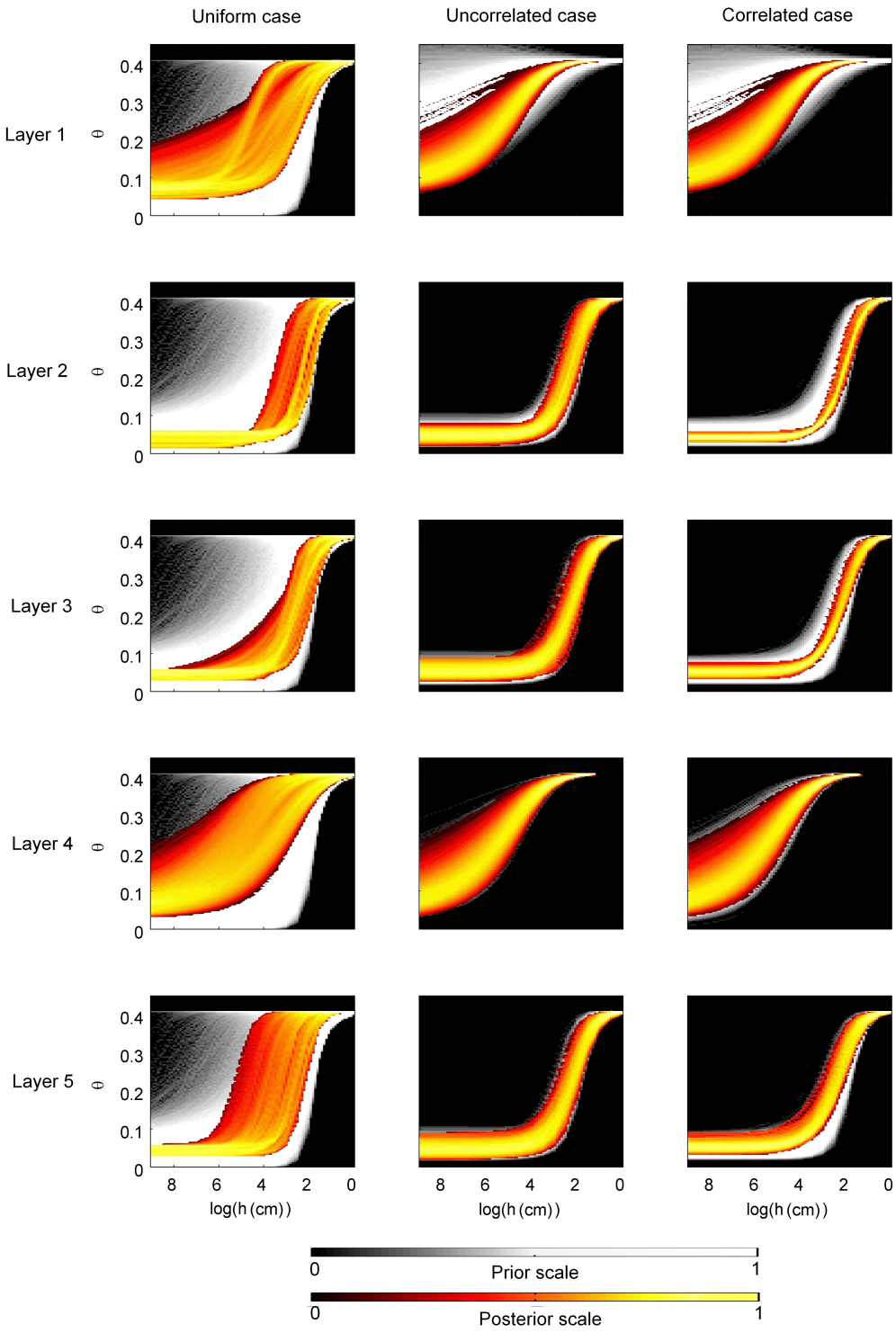

Figure 10: Water retention functions for each layer corresponding to the prior and posterior VGM parameter distributions shown in Figures 8 and 9.

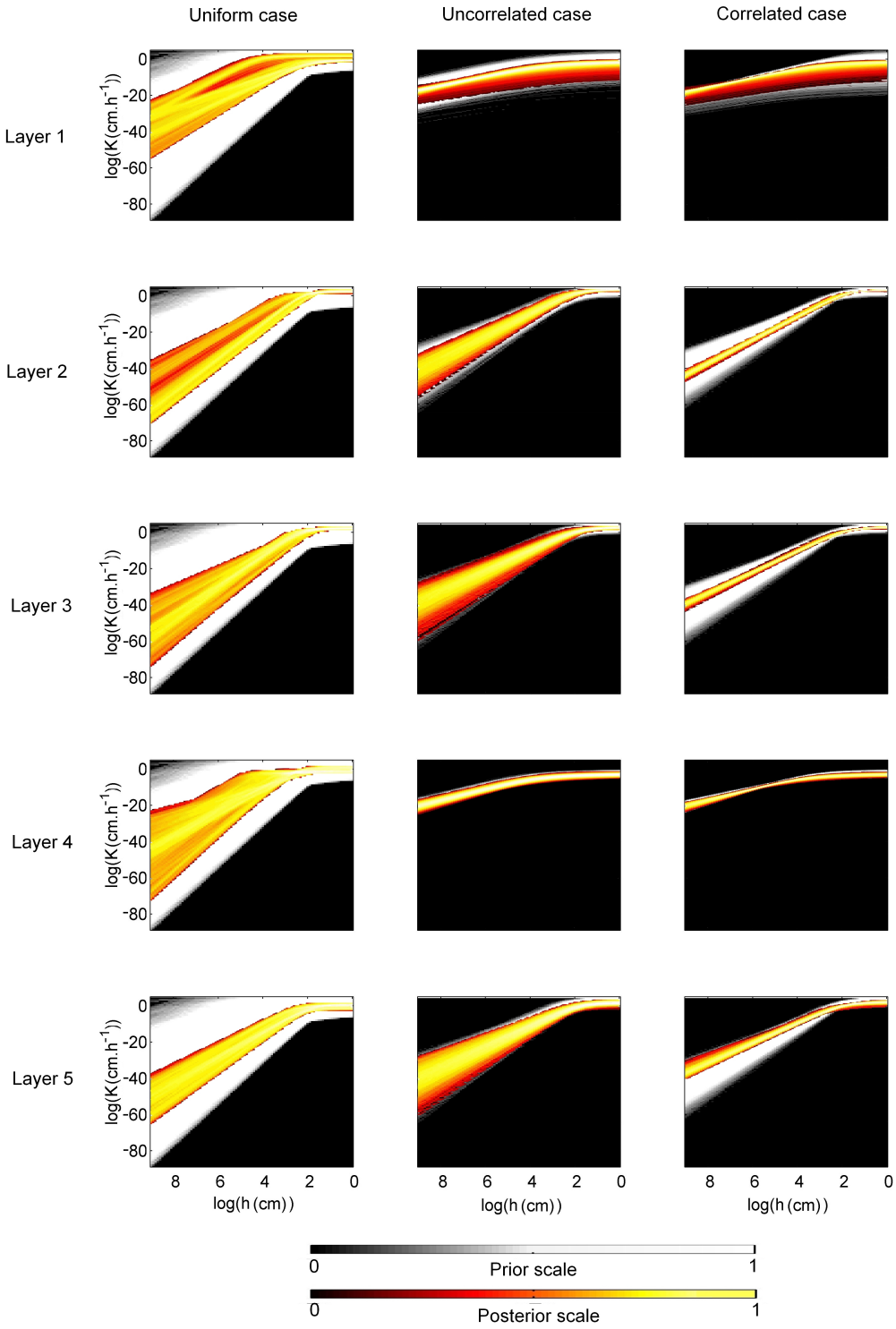

Figure 11: Hydraulic conductivity functions for each layer corresponding to the prior and posterior VGM parameter distributions shown in Figures 8 and 9.